Theory of fiber-optic, evanescent-wave spectroscopy and sensors

A. Messica, A. Greenstein, and A. Katzir

A general theory for fiber-optic, evanescent-wave spectroscopy and sensors is presented for straight, uncladded, step-index, multimode fibers. A three-dimensional model is formulated within the framework of geometric optics. The model includes various launching conditions, input and output end-face Fresnel transmission losses, multiple Fresnel reflections, bulk absorption, and evanescent-wave absorption. An evanescent-wave sensor response is analyzed as a function of externally controlled parameters such as coupling angle, f number, fiber length, and diameter. Conclusions are drawn for several experimental apparatuses. © 1996 Optical Society of America

1. Introduction

In the last decade fiber-optic, evanescent-wave spectroscopy (FEWS) has become a popular analytical method for IR absorbance spectroscopy.[1] FEWS is based on the attenuated total-internal-reflection (TIR) effect[2] and uses IR transparent optical fibers as sensing elements. This method has the advantages of fast, real-time, *in situ,* selective, nondestructive, and safe detection. It has been successfully employed in a variety of configurations for studies of solid–liquid interfaces,[3] chemical reaction rates,[4] complex material curing,[5] organometallic thin films,[6] liquid[7–10] and gas[11–15] detection and monitoring, concentration measurements,[16–19] and biological applications.[20,21] Usually the sensing elements are installed in a Fourier-transform IR (FTIR) spectrometer system, but recently tunable lasers were incorporated into FEWS systems[10,22] instead of conventional blackbody sources. This has improved the wavelength resolution, sensitivity, and detection limit of the method.

Although there have been much progress and an increase in published research, no complete theoretical formulation of this subject exists in the literature. Although wave-optics theory for single-mode fibers has been developed to give an accurate description, this is not the case for multimode optical fibers. From the early research of Elsasser[23–25] one can understand that an accurate solution of the wave equation for a multimode fiber is not applicable even when a powerful computer is used; therefore one must resort to a geometric optics description. Kapany and co-workers[26–29] and Potter[30,31] set the frame, within the framework of geometric optics, for a three-dimensional (3D) description of waveguide properties of optical fibers but did not consider attenuated TIR losses specifically. Because FEWS is based on the attenuated TIR effect, one must develop an appropriate description for light–matter interaction at the fiber–sample interface. Such a description was developed for planar waveguides[2,32–34] and optical fibers[35–38] mostly within the framework of wave-optics approximations. Recently there has been a great amount of theoretical research supported by experiments and devoted to FEWS sensors. This research gives a good description of attenuated TIR, both by wave-optics approximations[7,37] and by a two-dimensional (2D) geometric optics approach,[1,8,19,22] but does not provide a full description that takes into account additional factors that affect FEWS sensors such as launching conditions.

We present a comprehensive formulation of FEWS in general and fiber sensors based on the attenuated TIR effect specifically.[2] An extended formulation is devoted to different launching conditions that are found to be especially important for the detection properties of FEWS sensors. In Section 2 a generic 3D optical geometry model for bound and skew rays is formulated. Apart from various launching conditions the model accounts for input and output Fres-

The authors are with the Raymond and Beverly Sackler Faculty of Exact Sciences, School of Physics and Astronomy, Tel Aviv University, Tel Aviv 69978, Israel. A. Messica is currently at the Weizmann Institute of Science, Braun Center for Semiconductor Submicron Research, Rehovot 76100, Israel.

Received 25 July 1995; revised manuscript received 24 October 1995.

0003-6935/96/132274-11$10.00/0

nel transmission, multiple Fresnel reflections at both fiber end faces, and bulk and evanescent-wave absorption. In Section 3 we present results for different sensor configurations as a function of controlled parameters such as coupling angle, spot size, fiber length, and diameter. In Section 4 we discuss the results and measures that can be taken to optimize the FEWS performance. In Section 5 we summarize the main results of this study and conclude with some remarks regarding the model, the numerical simulations, and the role of the model in the design and practice of FEWS.

2. Theoretical Model

Let us consider an ideal straight, uncladded, step-index, multimode fiber, not restricted to weak guidance, for which the V number $[V \equiv (2\pi a/\lambda)(n_{co}^2 - n_{cl}^2)]$ is much higher than unity. Here a is the fiber radius, λ is the wavelength, and n_{co} and n_{cl} are the fiber core and clad refractive indices, respectively. Ray optics is a good approach to considering these fibers, providing an intuitive and fairly accurate analytical solution compared with the wave-optics approach. Our purpose is to determine the power transmittance, guided along the fiber by bound and tunneling skew rays. We assume an arbitrary intensity angular distribution, $I(r, \gamma, \theta, \varphi)$, at the fiber-input end face. Angles θ and φ define solid angle $d\Omega$, r and γ define an area element, dS, at the fiber-input end face as depicted in Fig. 1(a). The general expression for P, the total power transmitted by an optical fiber[30,31] of length L and radius a, is

$$P(L, a) = \iint T(r, \gamma, \theta, \varphi) * I(r, \gamma, \theta, \varphi) dS d\Omega, \quad (1)$$

where T is a general transmission function whose form depends on fiber-optic properties and ray direction. T is composed of several factors, e.g., Fresnel transmissions at the fiber end faces, multiple reflections from both fiber end faces, bulk absorption, and attenuated TIR. In Subsections 2.A–2.E we give a detailed description of these factors and a full representation of T at the end. Various launching conditions manifest themselves through I. Angles θ and φ have the same meaning as in spherical coordinates, and the coordinate system is chosen so that θ is the inclination angle with respect to the axial direction [see Fig. 1(a)]. Equation (1) assumes no coherent propagation and therefore contains no phase information. The integral is over the intensity of each guided ray, and no possible interference is taken into account.

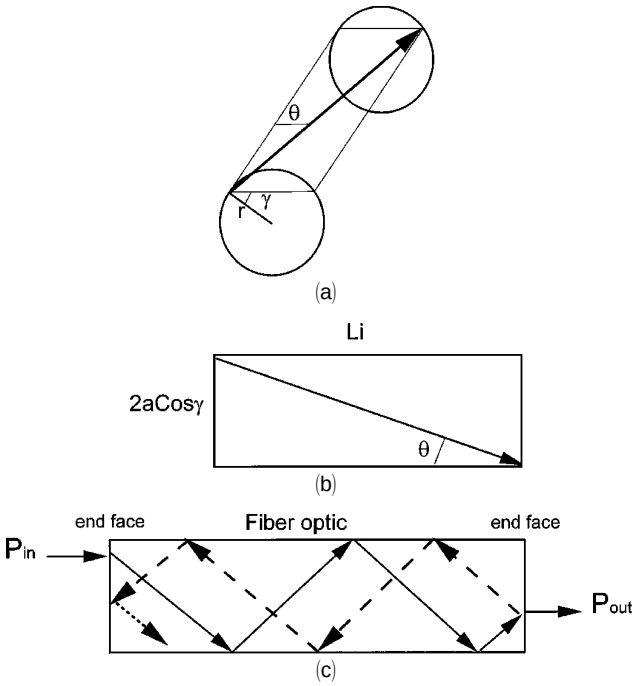

Fig. 1. Schematic view of ray propagation: (a) Propagation plane defined by γ, the skewness angle, and, θ, the axial angle; (b) top view of the propagation plane; (c) multiple Fresnel reflections at the fiber end faces.

A. Conditions for Bound and Tunneling Skew-Ray Propagation

Each guided ray is characterized by axial angle θ and by γ, a skewness angle between the fiber radius and the normal at the point of incidence. These angles define a plane in which a skew ray propagates. From geometry one may verify that in three dimensions one must modify Snell's law for TIR in the following manner[30,31,36]:

$$\sin\theta \cos\gamma \le [1 - (n_{cl}^2/n_{co}^2)]^{1/2}. \quad (2)$$

For $\gamma = 0$ one obtains the well-known and familiar expression for the TIR critical angle in the 2D description. The maximal value θ_M possible for θ, the axial angle, is given by applying Snell's law for a ray that is incident on the fiber input at grazing incidence $\theta' = 90°$:

$$\sin\theta_M = n_{air}/n_{co}. \quad (3)$$

Note that by inequality (2) in the 3D case a TIR is possible even for angles greater than the 2D critical angle defined by $\sin\theta_c = [1 - (n_{cl}^2/n_{co}^2)]^{1/2}$.

Thus the allowed values for γ are

$$\begin{aligned} 0 \le \theta \le \theta_c &\Rightarrow 0 \le \gamma \le 90°, \\ \theta_c \le \theta \le \theta_M &\Rightarrow \gamma_m \le \gamma \le 90°, \end{aligned} \quad (4)$$

where $\cos\gamma_m \equiv \sin\theta_c/\sin\theta$, which means that for any inclination angle in the $\theta_c \le \theta \le \theta_M$ range skewness angle γ has lower bound γ_m. It is clear that if $\theta_M > \theta_c$, the integral over the solid angle is divided into two integrals and the limits are determined according to inequalities (4).

B. Fresnel Reflections at the Fiber End Faces

To take into account the total power transmission of a FEWS system, one must consider the passage of

rays into and out of the fiber. Therefore transmission function T should contain the Fresnel transmission coefficients for the fiber input and output end faces. Because of its helical path a skew ray does not have a definite polarization; hence the transmitted power is equally weighted over the two possible polarizations. The Fresnel transmission coefficients are determined by θ, the incidence angle, irrespective of skewness angle γ and by the fiber and air refractive indices, which are given by[2,23,24,36]

$$t^2 = \tfrac{1}{2}(t_p^2 + t_s^2), \tag{5}$$

where the Fresnel power transmission coefficients[23] are given, by Snell's law, as

$$t_p^2 = \frac{4n_{co}\cos\theta \times b}{(n_{co}\cos\theta + b)^2}, \qquad t_s^2 = \frac{4n_{co}n_{air}\cos\theta \times b}{(n_{air}^2\cos\theta + n_{co}b)^2},$$
$$b \equiv (n_{air}^2 - n_{co}^2\sin^2\theta)^{1/2}. \tag{6}$$

C. Bulk and Evanescent-Wave Absorption

Bulk absorption attenuates the power carried by each guided ray, traversing a fiber of length L and radius a, according to Beer–Lambert's law. Each guided ray undergoes N attenuated TIR's.[30,31] From Fig. 1(b) (top view of the propagation plane) it is clear that

$$N = \frac{L\tan\theta}{2a\cos\gamma}. \tag{7}$$

The path length each ray traverses between two successive internal reflections is

$$L_i = \frac{2a\cos\gamma}{\sin\theta}. \tag{8}$$

The total effective optical path is independent of skewness angle γ:

$$L_p = N \times L_i = \frac{L}{\cos\theta}. \tag{9}$$

The expression for bulk absorption is therefore $\exp(-\alpha_{co}L_p)$, where α_{co} is the bulk absorption coefficient.

Attenuated TIR occurs on each reflection at the fiber–sample interface. Note that the fiber is uncladded; hence the sample actually has the role of a lossy cladding (as long as its thickness is greater than the wavelength).

Once again, equal weight is assumed for two possible polarizations[36]:

$$r_{ATR}^2 = \tfrac{1}{2}(r_s^2 + r_p^2). \tag{10}$$

Then, employing Fresnel reflection coefficients for a ray that is incident on the boundary between the fiber and a lossy cladding (i.e., sample), we can write down, in the local plane-wave approximation[36] and in the limit of weak attenuated TIR, the evanescent-wave absorption expressions for each polarization:

$$r_s^2 = 1 - \frac{4n_{co}n_{cl}^2\cos\psi\left(\frac{\kappa_{cl}}{n_{cl}} - \frac{\kappa_{co}}{n_{co}}\right)}{(n_{co}^2 - n_{cl}^2)(n_{co}^2\sin^2\psi - n_{cl}^2)^{1/2}},$$
$$r_p^2 = 1 - \frac{4n_{co}^2n_{cl}^2\cos\psi\left(\frac{\kappa_{cl}}{n_{cl}} - \frac{\kappa_{co}}{n_{co}}\right) \times (2n_{co}^2\sin^2\psi - n_{cl}^2)}{(n_{co}^2 - n_{cl}^2)(n_{co}^2\sin^2\psi - n_{cl}^2)^{1/2} \times (n_{co}^2\sin^2\psi - n_{cl}^2\cos^2\psi)}, \tag{11}$$

where $\cos\psi = \sin\theta\cos\gamma$ and $\kappa_i = \alpha_i\lambda/4\pi$ so that index i stands for core or clad and α the usual nomenclature for the absorption coefficient. An explicit derivation of these expressions is in Appendix A. At this stage we are in a position to write the evanescent-wave absorption contribution to T. This is just $(r_{ATR}^2)^N$. This is the most important part of this study because all the spectroscopic information is contained within Eqs. (11) whereas all others may be normalized experimentally. Because Eqs. (11) express the reflected power on each reflection at the core–sample interface, one can intuitively regard the second term of the right-hand side as the power fraction evanescently absorbed by the sample. Note that, unlike transmission spectroscopy, when the Beer–Lambert law is obeyed, FEWS does not have a simple exponential form. Rather the complicated dependence on wavelength, absorption coefficients, and refractive indices gives, in general, a line shape different from that recorded by transmission spectroscopy.

D. Multiple Successive Reflections at Fiber End Faces

Each ray incident on the fiber output end face is partially backreflected. Figure 1(c) illustrates the process of multiple successive reflections at both fiber end faces. Each ray propagating to and fro undergoes bulk absorption and attenuated TIR losses. Considering these successive reflections, it is simple to make the summation and write the outcome:

$$M(\theta, \gamma) = 1 - [r^4 \times (r_{ATR}^2)^N\exp(-\alpha_{co}L_p)]^2. \tag{12}$$

Here r^2 is the power reflected from both fiber end

faces at the multiple-reflections path and has the same form as Eq. (10).

These reflection coefficients are taken as[23,24,36]

$$r_s^2 = \left[\frac{n_{co}\sin\psi - (n_{air}^2 - n_{co}^2\cos^2\psi)^{1/2}}{n_{co}\sin\psi + (n_{air}^2 - n_{co}^2\cos^2\psi)^{1/2}}\right]^2,$$

$$r_p^2 = \left[\frac{n_{air}^2\sin\psi - n_{co}(n_{air}^2 - n_{co}^2\cos^2\psi)^{1/2}}{n_{air}^2\sin\psi + n_{co}(n_{air}^2 - n_{co}^2\cos^2\psi)^{1/2}}\right]^2. \quad (13)$$

Here we emphasize that, although considered, this factor hardly affects the total power transmission as one would *a priori* suspect.

E. Launching Conditions

Coupling radiation into the fiber is usually performed by positioning the fiber input end face in focal plane f of a mirror or a lens. The simplest launching condition that we can think of we term a nontilted fiber and a centered spot, i.e., one in which the fiber and the coupling lens are aligned on the same optical axis and the spot center is located at the fiber-input end-face center ($\theta_s = 0$). This launching condition is primarily employed in FTIR FEWS. If the focused spot has a relatively large diameter, compared with the fiber diameter, such a launching condition excites both meridional and skew rays. A more general launching condition, which we call a tilted fiber and a centered spot, is one in which the fiber axis makes an angle, $\theta_s \neq 0$, with respect to the optical axis as depicted in Fig. 2. Such a launching condition is primarily employed in laser FEWS. Because the focused laser spot diameter is relatively small, the former launching condition excites primarily meridional or nearly meridional rays and the system response might be low. Hence tilted coupling is employed so as to enlarge the axial angle to enhance evanescent-wave absorption. Figure 2 illustrates the setup that is considered in the following formulation of a general tilted coupling. The last launching condition we consider is a variation of the preceding two, namely, a nontilted fiber and an off-centered spot. We are not familiar with reports regarding this launching condition; nevertheless we consider it because it enables the excitment of skew rays alone and therefore could be of great importance in FEWS sensors. Here we stress that the launching condition has an important effect on FEWS performance and therefore is the most important factor of all.

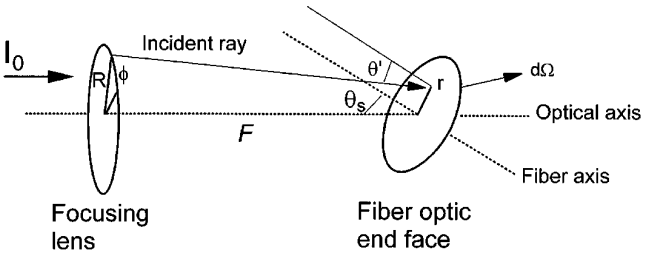

Fig. 2. Tilted fiber and centered-spot launching conditions: θ_s, angle between the optical axis and the fiber axis; θ', angle of incidence.

Let us consider a uniformly illuminated focusing lens and fiber positioned at its focal plane with a θ_s tilting angle. To calculate the intensity $I(\theta')$ distribution (the prime stands for the intensity distribution in the medium outside the fiber input, usually air) of each area element of the fiber input end face, we convert the radial integration at the lens plane in the following way:

$$I(\theta')d\theta' = \int_0^{2\pi} I_0 r'(\theta', \phi')dr'd\phi', \quad (14)$$

where I_0 is the intensity incident on the lens, $r'dr'd\phi'$ is an area element in the lens plane, and $r'(\theta', \phi')$ is given by

$$r'(\theta', \phi') = r\cos\phi' \pm [F(\theta') - r^2\sin^2\phi']^{1/2}, \quad (15)$$

$$F(\theta') \equiv \frac{f^2\sin^2(\theta' - \theta_s)}{\cos^2\theta'}. \quad (16)$$

The positive root is taken for $-\pi/2 \leq \phi' \leq \pi/2$ and the negative one for $\pi/2 \leq \phi' \leq 3\pi/2$.

Note that ϕ' is an azimuthal angle in the plane of the lens, but it also defines the angle between the projection of r' in the lens plane and r, the radial position of the incident ray at the fiber input. $I(\theta')$ is the intensity distribution incident on the fiber-input end face and is related to intensity distribution $I(\theta)$ inside the fiber when a Jacobian transformation through Snell's law is employed. Hence, given the angular intensity distribution outside the fiber-input end face, one may transform to the angular intensity distribution inside the fiber by

$$I(\theta) = I(\theta')\frac{n_{co}^2\cos\theta}{b}. \quad (17)$$

Note that $I(\theta)$ does not depend on fiber length[22] as long as $L \leq L_c \cong 1/\alpha_{co}$. For fibers longer than coupling length L_c, scattering mechanisms induce mode mixing that redistributes the direction of the ray (and power). At that point the ideal fiber assumption is no longer valid, and one must take this into account through modification of $I(\theta) = I(\theta, L)$.

Experimentally, the tilting angle may be changed to optimize the system response in terms of evanescent absorption and signal-to-noise (S/N) considerations. Another important fact is that for a narrow-angular-width coupling, as is the case for laser FEWS, one may well approximate the incident intensity distribution by a constant. Last, to enhance evanescent absorption, one may want to launch skew rays alone by coupling to $\gamma_m \leq \gamma \leq 90°$ angles. Experimentally this can be done with a spatial filter positioned at the entrance cone. The experimentalist who wants to avoid introducing this filter can circumscribe spatial filtering by considering a spot that is focused in an offset position on the fiber-input

end face; i.e., the spot center is located a distance r_0 from the input end-face center. Analytically this kind of launching condition manifests as a change in the integration limits of the r, ϕ, and γ variables. Expressions for the integration limits and area elements of the different launching conditions are given in Appendix B.

Note that from the launching condition point of view, employing lasers in FEWS is far superior to conventional blackbody sources, such as those employed in FTIR or other spectrometers. This is due to the narrow beamwidth and angular distribution that enable better control of experimental conditions such as sensor response or signal-to-noise constraints.

To conclude and summarize, we have presented a general 3D model for a FEWS system. The different launching conditions, input and output Fresnel transmission, multiple Fresnel reflections, and bulk and evanescent-wave absorption, have been formulated explicitly, giving the main result for transmission function T:

$$T(r, \gamma, \theta, \varphi) = \frac{t^4 (r_{\mathrm{ATR}}{}^2)^N \exp(-\alpha_{\mathrm{co}} L_p)}{M(\gamma, \theta)} . \qquad (18)$$

The numerical calculation of the integral defined in Eq. (1) is therefore straightforward.

3. Results

Three different apparatuses, A–C in our nomenclature, were considered, and parameters were taken from experimental data.[10,15,18] The integration of Eq. (1) was carried out along the following lines with an eight-point Gauss–Legendre integration scheme. The evanescent-wave absorption, $A \equiv -\ln(T_{\mathrm{sample}}/T_{\mathrm{background}})$, was calculated in a manner that matches the experimental procedure. First, the fiber transmission was calculated without the presence of the sample (which we term a background measurement, i.e., $\kappa_{\mathrm{cl}} = 0$), and then the fiber transmission was calculated with the sample present (termed a sample measurement, e.g., for a gas or a liquid, κ_{cl} = finite and small). Evanescent-wave absorption A is therefore calculated as a function of externally controlled parameters and presented for the three apparatuses described below. Experimental parameters[15] used for the calculation of SF_6 gas absorption were $n_{\mathrm{air}} = 1$, $n_{\mathrm{co}} = 2.15$, $\lambda = 10.562$ μm, $\alpha = 0.05$ cm^{-1}, $\kappa_{\mathrm{cl}} = 0.0307$, $\theta_s = \pi/9$.

A. Laser FEWS Tilted Fiber and Centered Spot Configuration

For evanescent-wave sensors based on laser sources[10] the common practice is to launch laser radiation at angle θ_s with respect to the fiber axis. Because laser sources excite a relatively low number of modes with a narrow axial angle spread, then for the $\theta_s = 0$ case, the evanescent absorption response is low. Therefore it is useful to employ a tilted coupling to improve evanescent-wave absorption. This procedure, easily performed experimentally, usually improves evanescent-wave absorption without signal-to-noise degradation.

B. FTIR FEWS Nontilted Fiber and Centered-Spot Configuration

For an FTIR FEWS apparatus a common practice is to focus the blackbody source 's radiation onto the fiber-input end face by a coupling lens with a large f number (F#), e.g., 1, to maintain a reasonable S/N ratio (~100). The source, the coupling lens, and the optical fiber are all aligned to the same optical axis. Therefore this kind of coupling involves, relatively speaking, a wide entrance cone as does the spread in the axial angle.

C. Laser FEWS Nontilted Fiber and Off-Centered Spot Configuration

The third and last apparatus considered has never been reported on, as far as we know. We analyze it to check the effect of skew-ray-based coupling in FEWS systems. The excitation of skew rays alone can be achieved by focusing the beam to an off-center position on the fiber-input end face. We computed the evanescent-wave absorption of an off-centered focused spot of a laser FEWS sensor for the nontilted fiber case, i.e., $\theta_s = 0$ and took $r_0 = a/2$ in all calculations.

Figure 3 presents evanescent-wave absorption as a function of fiber length for the three different launching configurations. A remarkable linear dependence of absorbance versus fiber length is evident. This indicates that fiber transmission is an exponential decaying function of the fiber length usually characteristic of transmission spectroscopy.

Figures 4 and 5 are closely related because both depict the tilting angle dependence of the two major FEWS systems employed currently, i.e., A and B configurations. Figure 4 presents the laser FEWS,

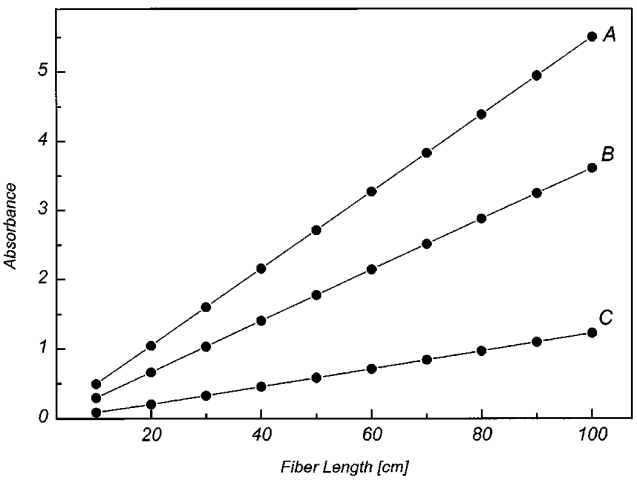

Fig. 3. Evanescent-wave absorbance versus fiber length for three different experimental apparatuses. A, laser FEWS of a tilted fiber and centered-spot coupling; B, FTIR FEWS of a nontilted fiber and a centered spot; C, laser FEWS for a nontilted fiber and an off-centered spot.

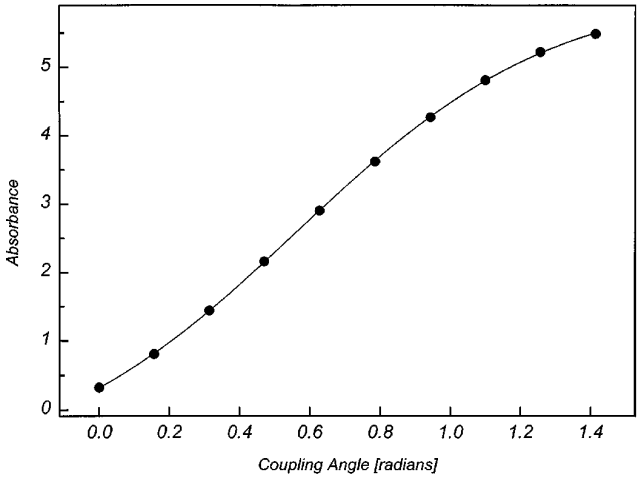

Fig. 4. Evanescent-wave absorbance versus coupling angle for a laser FEWS sensor with centered-spot coupling.

configuration A, evanescent-wave absorbance as a function of tilting angle. Note that in this case the fiber and the coupling lens are positioned to make angle θ_s between their optical axes. The laser FEWS sensor exhibits a sigmoid behavior in general and a parabolic one for low values of θ_s. An approximate linear region exists in the $0.3 \leq \theta_s \leq 0.8$ range and is important for practical applications when measurement repeatability is crucial and one wants to maintain high precision. Therefore coupling the laser radiation at angles in this regime overcomes nonlinearity in the sensor response to this external parameter. In fact the coupling angle can be changed easily and tuned as a preliminary step for S/N optimization before measurement. Therefore it serves as a convenient external controlling parameter and may improve system performance if one takes into account its response curve.

Figure 5 depicts a similar calculation for a FTIR FEWS, configuration B, but now the evanescent absorbance is calculated versus the lens F#. Here we change the entrance cone of the radiation focused onto the fiber-input end face. Therefore the high values of F# in Fig. 5 correspond to large entrance cones and vice versa. A parabolic dependence of the system response curve can be observed, which is compatible with recent reports.[19,39]

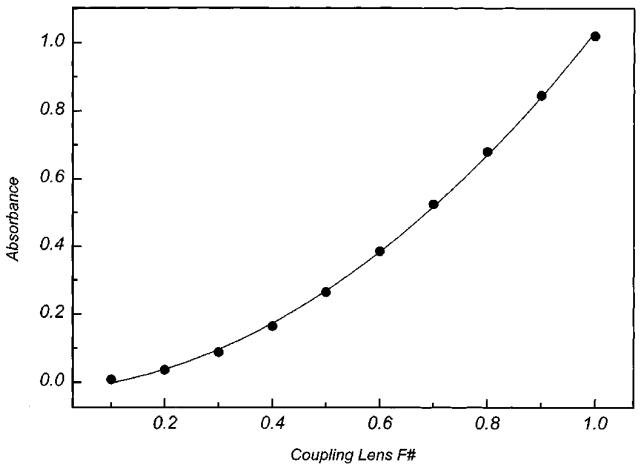

Fig. 5. Evanescent-wave absorbance versus coupling lens F# for a FTIR FEWS apparatus with centered-spot coupling.

Figure 6 depicts the evanescent-wave absorbance versus fiber radius for the three different configurations discussed. Here also we find that the laser FEWS tilted fiber and centered spot configuration feature the best performance. In terms of sensor sensitivity both A and B configurations exhibit a similar performance, but the detection limit of the former is better. The laser FEWS nontilted fiber and off-centered spot, the C configuration, is inferior to both.

4. Discussion

The pseudo-Beer–Lambert behavior observed is not intuitive because, as argued above, FEWS transmission does not in general possess a simple exponential form. The linear absorbance versus length dependence may be expected for laser FEWS sensors, because with these sensors all laser energy is launched within a very narrow (a few degrees) entrance cone and a relatively small spot size. Therefore rays excited inside the fiber suffer similar absorption, effectively making the sensor obey a pseudo-Beer–Lambert law. Such behavior for laser FEWS sensors has been predicted both by 2D (Ref. 22) and by 3D (Ref. 10) models. Note that configuration A (the laser FEWS tilted fiber and centered spot) is superior to both other configurations in terms of sensitivity and detection limit. The linear dependence of the FTIR FEWS apparatus is in contrast to 2D model predictions[10,22] and has been verified experimentally.[19] Although one could think that by coupling to skew rays alone, the C configuration, the number of reflections [Eq. (7)] each ray suffers at the fiber–sample interface is increased, therefore increas-

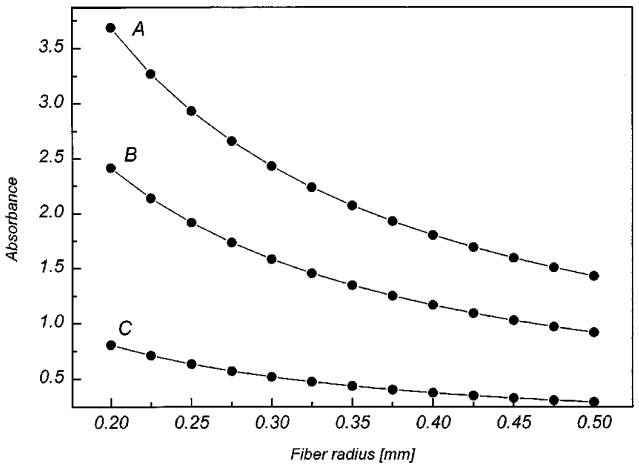

Fig. 6. Evanescent-wave absorbance versus fiber radius for three different FEWS apparatuses: A, laser FEWS of a tilted fiber and centered-spot coupling; B, FTIR FEWS of a nontilted fiber and a centered spot; C, laser FEWS for a nontilted fiber and an off-centered spot.

ing sensor sensitivity and detection limit. This is more than compensated when the low axial angle is excited, thus degrading sensor performance. This might drastically change if one couples radiation at a modified C configuration of an off-centered position with a tilting angle, but it may turn out to be difficult to utilize and optimize experimentally.

In terms of absolute absorbance, FTIR FEWS is inferior to laser FEWS. This is due to the large entrance cone, because different rays suffer different evanescent absorption. Rays excited at low axial angles suffer little absorption, rays excited at higher angles contribute more to the sensor response, but the overall absorption is averaged over all axial angles excited, resulting in reduced absorption, hence reduced response. For laser FEWS the equivalent cone angle carries all the energy and is therefore more efficient in terms of evanescent absorption. Moreover S/N consideration has not been taken into account. If one wants to couple radiation at a specific entrance angle with an iris or a spatial filter, the trade-off in the reduced signal intensity launched into the fiber will come into play and manifest itself as a reduced S/N leading to a degraded measurement precision. In this sense laser FEWS sensors have the advantage over FTIR sensors as reported by Schnitzer *et al.*[22] who applied a 2D model.[22] Needless to add is the fact that tuning the coupling angle in the laser FEWS sensor is by far easier than replacing the coupling lens in the FTIR FEWS.

From Fig. 6 one can deduce that a significant improvement in the sensor detection limit is obtained for all systems at a fiber radius smaller than 350 μm. This should be taken into account in view of coupling efficiency and convenience when one seeks to improve the detection limit by utilizing optical fibers of smaller diameter. Although the C configuration has an approximate linear response as a function of fiber radius, both of the other configurations have a $1/a$ dependence as recently reported by Katz *et al.*[19] This makes it beneficial to use fibers of smaller diameter because the overall amount of reflection each ray suffers at the fiber–sample boundary is increased, hence improving sensitivity and detection limit.

To gain more insight into the subject, we find it worthwhile to crunch mathematically integral (1) by making some crude approximations, obtaining a qualitative analytical expression for the absorbance. We focus on the two major FEWS apparatuses (A and B). Consider a laser FEWS apparatus with a centered spot and tilted fiber launching condition. Even for relatively high values of θ_s (but still far from θ_M) the axial angle is small enough that $\sin\theta \approx \theta$ and $\cos\psi \approx \sin\theta \approx \theta$. For the centered spot launching condition $\cos\gamma \approx 1$. To a reasonable approximation it can be shown that the multiple reflections term $M(\theta, \gamma)$, the Fresnel transmission coefficients, and the bulk absorption may be set as constants throughout the integration and can be factored out of integral (1).

If that is the case, the FEWS term may be approximated as follows:

$$(R_{\mathrm{ATR}})^N \sim (1 - K\theta)^N \sim \exp\left(-K\frac{L\theta^2}{2a}\right), \tag{19}$$

where K is a constant dependent on fiber and sample refractive indices and absorption constants.

The intensity distribution inside the fiber may be approximated as

$$I(\theta) \approx C(\theta - \theta_s), \tag{20}$$

where C is a constant dependent on the beam intensity, lens focal length, fiber and air refractive indices, and tilting angle.

Therefore it is possible to write an approximate expression for the relative transmittance of a FEWS sensor as

$$T(L, a) \propto \int \mathrm{d}\theta(\theta - \theta_s)\exp\left(-K\frac{L\theta^2}{a}\right). \tag{21}$$

The integration limits are $\theta_s - \delta \le \theta \le \theta_s + \delta$ for the laser FEWS and $0 \le \theta \le \theta_T$ for FTIR FEWS. θ_T defines the entrance cone of the FTIR system and δ the angular spread for the laser system, i.e., the wide and narrow entrance cones, respectively. Therefore for the laser FEWS system this integral may be approximated as

$$T(L, a, \theta_s) \propto \delta^2 \exp\left[-K\frac{L(\theta_s + \delta)^2}{a}\right]. \tag{22}$$

For the FTIR FEWS system one obtains

$$T(L, a, \theta_T) \propto \int_0^{\theta_T} \mathrm{d}\theta * \theta * \exp\left(-K\frac{L\theta^2}{a}\right), \tag{23}$$

which may be approximated to a similar result. Note that this crude approximation is reasonably compatible with the numerical results. One can easily calculate the absorbance and obtain linear dependence on fiber length, inverse dependence on fiber radius, and parabolic dependence for the tilting angle. This by no means is a trivial result. Usually one cannot factor out the contributing terms of integral (1). Hence one cannot expect such a response unless small values of the tilting angle are considered. For laser FEWS this condition is not always met, and indeed one can see that for high tilting-angle values this approximation fails to follow the sigmoid behavior that stems from numerical computations. For FTIR FEWS this approximation is fairly adequate even for a coupling lens with f/1. This is because the entrance cone angle, $\theta_T = \arctan(R_L/F)$, although relatively wide, still meets our constraint. We have also performed a numerical computation of Eq. (10) in this spirit, i.e., discarding the mentioned terms in the integration and obtaining similar results with a discrepancy of a few percent. Therefore one can use the approximation above for practical applications by employing a re-

verse engineering procedure to the experimental data with K as a fitting parameter. We emphasize that this approximation is valid only for the experimental parameters characterizing the experimental apparatus discussed and fail for an apparatus in which high tilting angles are involved. To conclude, let us point out that the absorbance is computed as a function of the relative transmittance, i.e.,

$$A \equiv -\ln\left[\frac{T(L, a, \theta_s, \kappa_{\mathrm{cl}})}{T(L, a, \theta_s, \kappa_{\mathrm{cl}} = 0)}\right].$$

Therefore numerically it is possible to obtain high absorbance values whereas experimentally the value of the numerator must exceed the system's noise. Therefore interpretation of the simulation results should always be made in view of S/N considerations that are closely connected with bulk absorption and always present. In fact S/N and bulk absorption limit our capability to enhance evanescent absorption with longer optical fibers. Therefore it is not possible to reach any desired detection limit by simply using longer sensors. Moreover the model is formulated in the geometric optics approach; thus it is not valid for fibers with radii smaller than 0.2 mm. For these diameters a local plane-wave approximation breaks down.

5. Summary

We have presented a comprehensive 3D model for a FEWS sensor based on straight, uncladded, step-index multimode optical fiber immersed in an absorbing media, i.e., a sample. The model takes into account contributions of Fresnel transmission coefficients at the fiber end faces, multiple reflections, bulk absorption, and most important evanescent-wave absorption and the various launching conditions usually employed. Our model indicates that, as indicated by experiment, one may disregard several terms and focus on evanescent-wave absorption and launching condition alone. In certain conditions it is possible to use an approximate expression, $A = K(L/a)\theta_s{}^m$, for the absorbance where $m \sim 2$ and K is a fitting parameter. Checking for conventional experimental setups, we find that a laser FEWS sensor with a tilted fiber launching condition has a better response than its FTIR counterpart. Both setups are superior, in terms of evanescent absorption response, to the off-centered spot and nontilted fiber laser configuration. Surprisingly, both FTIR and laser FEWS sensors feature a pseudo-Beer–Lambert dependence on fiber length. (Note that the fiber itself is not the absorbing medium.) We find that the evanescent-wave absorbance is inversely dependent on fiber radius and possesses almost a parabolic dependence on coupling angle. These may be optimized to enhance evanescent-wave absorption to improve the sensor performance in terms of sensitivity and detection limit. The use of this model is important for understanding, design, and construction of an optimal FEWS sensor for use in all fields of science, medicine, and industry.

Appendix A.

The Fresnel reflection coefficient of s (perpendicular, normal) polarization and p (parallel) polarization for a ray incident on the boundary between two media characterized by n_1 and n_2 refractive indices are

$$r_s = \frac{n_1 \sin\theta_i - n_2 \sin\theta_t}{n_1 \sin\theta_i + n_2 \sin\theta_t},$$
$$r_p = \frac{n_2 \sin\theta_i - n_1 \sin\theta_t}{n_2 \sin\theta_i + n_1 \sin\theta_t}, \tag{A1}$$

where θ_i is the incidence angle of a ray in a medium characterized by an n_1 refractive index and θ_t is the refracted angle in an n_2 medium. Because the reflected and refracted rays are coplanar, this description does not involve skewness angle γ; thus the generalization of Fresnel coefficients to the 3D fiber optic is straightforward. The coefficients above are given for the amplitude of the reflected wave. The power fraction reflected, which is of our interest, is the absolute square of these expressions. For TIR θ_t is imaginary but still may be expressed as

$$\cos\theta_t = i\,\frac{[\sin^2\theta_i - (n_2/n_1)^2]^{1/2}}{(n_2/n_1)}. \tag{A2}$$

Substituting Eq. (A2) into Eq. (A1), we obtain the Fresnel reflection coefficients for the TIR case:

$$r_s = \frac{n_1 \cos\theta_1 - i(n_1{}^2 \sin^2\theta_i - n_2{}^2)^{1/2}}{n_1 \cos\theta_1 + i(n_1{}^2 \sin^2\theta_i - n_2{}^2)^{1/2}},$$
$$r_p = \frac{n_2{}^2 \cos\theta_i - i(n_1{}^2 \sin^2\theta_i - n_2{}^2)^{1/2}}{n_2{}^2 \cos\theta_i + i(n_1{}^2 \sin^2\theta_i - n_2{}^2)^{1/2}}. \tag{A3}$$

From these equations we can understand that the absolute value of the reflection coefficients is always unity. Hence no attenuation occurs during reflection, i.e., TIR. Generalizing this formalism to account for losses in both media is done by assigning a complex value for refractive index $n(\lambda) \rightarrow n(\lambda) - i\kappa(\lambda)$. The imaginary part of the refractive index is proportional to absorption coefficient $\alpha(\lambda)$. Making this substitution into Eqs. (A3) gives the power fraction reflected for the attenuated TIR case:

$$|r_s|^2 = \left|\frac{(n_1 - i\kappa_1)\cos\theta_i - i[(n_1 - i\kappa_1)^2\sin^2\theta_i - (n_2 - i\kappa_2)^2]^{1/2}}{(n_1 - i\kappa_1)\cos\theta_i + i[(n_1 - i\kappa_1)^2\sin^2\theta_i - (n_2 - i\kappa_2)^2]^{1/2}}\right|^2,$$
$$|r_p|^2 = \left|\frac{(n_2 - i\kappa_2)^2\cos\theta_i - i(n_1 - i\kappa_1)[(n_1 - i\kappa_1)^2\sin^2\theta_i - (n_2 - i\kappa_2)^2]^{1/2}}{(n_2 - i\kappa_2)^2\cos\theta_i + i(n_1 - i\kappa_1)[(n_1 - i\kappa_1)^2\sin^2\theta_i - (n_2 - i\kappa_2)^2]^{1/2}}\right|^2. \tag{A4}$$

Although it is not too evident, studying these equations, we can figure that for incidence angles close to the critical angle the power reflection coefficients change abruptly. As far as low-loss fibers and weak attenuation are concerned, for incidence angles far from the critical angle it is possible to employ first-order approximations to these equations and gain some insight into the attenuated TIR effect.

In the following, we expand Eqs. (A4) to first-order terms in κ. We assume a low-loss fiber and a weak attenuated TIR so that the following conditions are valid:

$$\kappa_i \ll n_i \text{ for } i = 1, 2,$$
$$\frac{|n_2\kappa_2 - n_1\kappa_1 \sin^2\theta|}{|n_1^2 \sin^2\theta - n_2^2|} \ll 1 \tag{A5}$$

that usually hold for FEWS measurements. The i index that stands for incidence was omitted for clarity but should be considered as present.

On expanding the square root in Eqs. (A4), we make use of a complex functions theory that states that to express the form $(a + ib)^{1/2}$ the proper solution is

$$(a + ib)^{1/2} = x + iy, \tag{A6}$$

where x and y are

$$x = -\left[\left|\frac{a \pm (a^2 + b^2)^{1/2}}{2}\right|\right]^{1/2},$$
$$y = -\left[\left|\frac{-a \pm (a^2 + b^2)^{1/2}}{2}\right|\right]^{1/2}. \tag{A7}$$

In the conditions specified in (A5) and using a first-order expansion

$$\left[1 + \left(\frac{b}{a}\right)^2\right]^{1/2} \approx 1 + \frac{b^2}{2a^2},$$

we can write the approximations for x and y as

$$x \approx -\sqrt{a} = -(n_1^2 \sin^2\theta - n_2^2)^{1/2},$$
$$y \approx -\frac{b}{2\sqrt{a}} = -\frac{n_2\kappa_2 - n_1\kappa_1 \sin^2\theta}{(n_1^2 \sin^2\theta - n_2^2)^{1/2}}; \tag{A8}$$

then the final expression for $|r_s|^2$ is

$$|r_s|^2 = \left|\frac{(n_1 - i\kappa_1)\cos\theta + i(n_1^2 \sin^2\theta - n_2^2)^{1/2} - \dfrac{n_2\kappa_2 - n_1\kappa_1 \sin^2\theta}{(n_1^2 \sin^2\theta - n_2^2)^{1/2}}}{(n_1 - i\kappa_1)\cos\theta - i(n_1^2 \sin^2\theta - n_2^2)^{1/2} + \dfrac{n_2\kappa_2 - n_1\kappa_1 \sin^2\theta}{(n_1^2 \sin^2\theta - n_2^2)^{1/2}}}\right|^2. \tag{A9}$$

Taking the absolute value of Eq. (A9) and retaining only first-order terms of κ, we obtain

$$|r_s|^2 = \frac{(n_1^2 - n_2^2) - 2\cos\theta \dfrac{n_1 n_2 \kappa_2 - n_2^2 \kappa_1}{(n_1^2 \sin^2\theta - n_2^2)^{1/2}}}{(n_1^2 - n_2^2) + 2\cos\theta \dfrac{n_1 n_2 \kappa_2 - n_2^2 \kappa_1}{(n_1^2 \sin^2\theta - n_2^2)^{1/2}}}. \tag{A10}$$

Rearranging the nominator by subtraction and addition of the second term while neglecting the second term in the denominator with comparison to the first, we obtain the final result:

$$|r_s|^2 = 1 - \frac{4n_1 n_2^2\left(\dfrac{\kappa_2}{n_2} - \dfrac{\kappa_1}{n_1}\right)\cos\theta}{(n_1^2 - n_2^2)(n_1^2 \sin^2\theta - n_2^2)^{1/2}}. \tag{A11}$$

In a similar manner one may approximate the expression for $|r_p|^2$ given by Eqs. (11).

Appendix B.

Considering the general case of a tilted fiber and a centered spot, it is of great use to employ the polar representation for the ellipse, because the projection of the spot on the input endface is an ellipse with semiaxes $A = r_s/(\cos\theta_s)$ and $B = r_s$. Using $a \sin\gamma = r \sin\varphi$ between φ and γ, we write the area integration needed for Eq. (1) computation in terms of skewness angle γ:

$$\int_0^{\arcsin(B/a)} 4a\cos\gamma d\gamma \int_{a\sin\gamma}^{|A^2B^2 - (A^2 - B^2)a^2\sin^2\gamma|^{1/2}} \times \frac{r dr}{(r^2 - a^2\sin^2\gamma)^{1/2}}. \tag{B1}$$

The nontilted fiber and a centered spot launching condition is achieved by taking $\theta_s = 0$. The limits for the axial incidence angle are determined by

$$\frac{\pi}{2} < \phi' \le \frac{3\pi}{2}:$$
$$\frac{r}{f\cos\theta_s} \le \tan\theta' - \tan\theta_s \le \frac{(R_L^2 + r^2 - 2R_L r\cos\phi')^{1/2}}{f\cos\theta_s},$$
$$-\frac{\pi}{2} < \phi' \le \frac{\pi}{2}:$$
$$\frac{r}{f\cos\theta_s} \ge \tan\theta' - \tan\theta_s > \frac{r\sin\phi'}{f\cos\theta_s}$$
$$\frac{r\sin\phi'}{f\cos\theta_s} < \tan\theta' - \tan\theta_s \le \frac{(R_L^2 + r^2 - 2R_L r\cos\phi')^{1/2}}{f\cos\theta_s}. \tag{B2}$$

Conversion of θ' (the incidence angle) limits to θ (the ray propagation axial angle) is through Snell's law. R_L is the lens radius or the beam radius (for a collimated beam incident on the lens with a beam diameter smaller than the lens diameter). The limits for ϕ' are $[0, 2\pi]$.

Considering the case in which one desires to excite skew rays alone by an off-centered spot (no tilting angle), the integration limit for the skewness angle is determined by

$$\sin \gamma_{\min} = \frac{r_0 \sin \varphi - r_s}{r_0 \cos \varphi},$$
$$\sin \gamma_{\max} = \frac{r_0 \sin \varphi + r_s}{r_0 \cos \varphi}. \tag{B3}$$

Here (r_0, φ) is the vector position of the center of the off-centered spot and r_s is the spot radius.

The limits of the radial integration are given by

$$\tilde{R}_{\min}{}^2 = [r_0 \cos \varphi - [r_s{}^2 - (r_0 \sin \varphi - a \sin \gamma)^2]^{1/2}]^2 + a^2 \sin^2 \gamma,$$
$$\tilde{R}_{\max}{}^2 = [r_0 \cos \varphi + [r_s{}^2 - (r_0 \sin \varphi - a \sin \gamma)^2]^{1/2}]^2 + a^2 \sin^2 \gamma. \tag{B4}$$

The integration limits for the incidence angle are the same as above, given by (B2) with the difference that now the integration is performed with an area element:

$$dS = a \cos \gamma d\gamma \frac{\tilde{R} d\tilde{R}}{(\tilde{R}^2 - a^2 \sin^2 \gamma)^{1/2}}. \tag{B5}$$

Therefore one must transform r in Eq. (B2) by

$$r^2 = r_0{}^2 + \tilde{R}^2 - 2 r_0 \tilde{R} \cos(\varphi - \phi'), \tag{B6}$$

where $\tilde{R}$ denotes the radius vector to the incident position taken from the center of the input end face and r is the same taken from the center of the beam spot.

A. Messica thanks David and Suzan Messica for support. This research is dedicated to the memory of B. Bar.

References

1. S. Simhony, E. M. Kosower, and A. Katzir, "Novel attenuated total internal reflectance spectroscopic cell using infrared fibers for aqueous solutions," Appl. Phys. Lett. **49,** 253–254 (1986).
2. N. J. Harrick, *Internal Reflection Spectroscopy* (Wiley, New York, 1967); M. Mirabella and N. J. Harrick, *Internal Reflection Spectroscopy Review and Supplement* (Harrick Scientific Corporation, New York, 1985).
3. R. Iwamoto and K. Ohta, "Quantitative surface analysis by Fourier transform attenuated total reflection infrared spectroscopy," Appl. Spectrosc. **38,** 359–365 (1984).
4. E. Margalit, H. Dodiuk, E. M. Kosower, and A. Katzir, "Infrared fiber evanescent wave spectroscopy for in-situ monitoring of chemical processes," in *Infrared Fiber Optics,* J. A. Harrington and A. Katzir, eds., Proc. Soc. Photo-Opt. Instrum. Eng. **1048,** 145–152 (1989).
5. N. A. Wright, R. Curbelo, D. A. C. Compton, and S. L. Hill, "The use of mid-infrared optical fibers for analytical applications," in *Infrared Fiber Optics,* J. A. Harrington and A. Katzir, eds., Proc. Soc. Photo-Opt. Instrum. Eng., **1048,** 153–161 (1989).
6. I. Feinstein-Jaffe, A. Borenstein, and M. Katz, "Fiber optic attenuated reflection spectroscopy (FO-ATR) for investigation of organometallic polymeric films," J. Am. Chem. Soc. **113,** 7042–7044 (1991).
7. P. H. Paul and G. Kychakoff, "Fiber-optic evanescent field absorption sensor," Appl. Phys. Lett. **51,** 12–14 (1987).
8. S. Simhony, I. Schnitzer, A. Katzir, and E. M. Kosower, "Evanescent wave infrared spectroscopy of liquids using silver halide optical fibers," J. Appl. Phys. **64,** 3732–3734 (1988).
9. K. Newby, W. M. Reichert, J. D. Andrade, and R. E. Benner, "Remote spectroscopic sensing of chemical adsorption using a single multimode optical fiber," Appl. Opt. **23,** 1812–1815 (1984).
10. A. Messica, A. Katzir, U. Schiessl, and M. Tacke, "Liquid and gas fiber-optic evanescent-wave spectroscopy by tunable lasers," in *Infrared Fiber-Optics III,* J. A. Harrington and A. Katzir, eds., Proc. Soc. Photo-Opt. Instrum. Eng. **1591,** 192–200 (1991).
11. H. Tai, H. Tanaka, and T. Yoshino, "Fiber-optic evanescent-wave methane gas sensor using optical absorption for the 3.392-μm line of a He–Ne laser," Opt. Lett. **12,** 437–439 (1987).
12. J. F. Giuliani, H. Wohltjen, and N. L. Jarvis, "Reversible optical waveguide sensor for ammonia vapors," Opt. Lett. **8,** 54–56 (1983).
13. V. Ruddy, S. MacCabe, and B. D. MacCraith, "Detection of propane by IR-ATR in a Teflon clad fluoride glass optical fiber," Appl. Spectrosc. **44,** 1461–1463 (1990).
14. S. J. Saggese, J. A. Harrington, and G. H. Sigel, "Hollow waveguides for sensor applications," in *Chemical, Biochemical, and Environmental Fiber Sensors II,* R. A. Lieberman and M. T. Wlodarczyk, eds., Proc. Soc. Photo-Opt. Instrum. Eng. **1368,** 2–14 (1991).
15. A. Messica, A. Greenstein, A. Katzir, U. Schiessl, and M. Tacke, "A fiber-optic evanescent-wave sensor for gas detection," Opt. Lett. **19,** 1167–1169 (1994).
16. Y. Mendelson, B. Y. Lin, R. A. Peura, and A. C. Clermont, "Carbon dioxide laser based multiple ATR technique for measuring glucose in aqueous solutions," Appl. Opt. **27,** 5077–5080 (1988).
17. D. Bunimovich, R. Kellner, R. Krska, A. Messica, I. Paiss, U. Schiessl, M. Tacke, K. Taga, and A. Katzir, "A system for monitoring and control of processes based on IR fibers and tunable diode lasers," J. Mol. Struct. **292,** 125–132 (1993).
18. R. Krska, E. Rosenberg, K. Taga, R. Kellner, A. Messica, and A. Katzir, "Polymer coated silver halide infrared fibers as sensing devices for chlorinated hydrocarbons in water," Appl. Phys. Lett. **61,** 1778–1780 (1992).
19. M. Katz, A. Borenstein, I. Schnitzer, and A. Katzir, "Attenuated total reflection spectroscopy with chalcogenide fiber," in *Infrared Fiber-Optics III,* J. A. Harrington and A. Katzir, eds., Proc. Soc. Photo-Opt. Instrum. Eng. **1591,** 236–246 (1991).
20. J. D. Andrade, R. A. Van Wagenen, D. E. Gregonis, K. Newby, and N. J. Lin, "Remote fiber-optic biosensors based on evanescent excited fluoroimmunoassay: concept and progress," IEEE Trans. Electron. Devices **32,** 1175–1179 (1985).
21. T. Vo-Dinh, B. J. Tromberg, G. D. Griffin, K. R. Ambrose, M. J. Sepaniak, and E. M. Gardenhire, "Antibody-based fiber-

optics biosensor for the carcinogen benzo(a)pyrene," Appl. Spectrosc. **41,** 735–738 (1987).
22. I. Schnitzer, A. Katzir, U. Schiessl, W. J. Riedel, and M. Tacke, "Evanescent field IR spectroscopy using optical fibers and tunable diode lasers," Mater. Sci. Eng. **B5,** 333–337 (1989).
23. J. A. Stratton, *Electromagnetic Theory* (McGraw Hill, New York, 1941), Sec. 9.4–9.8.
24. S. A. Schelkunoff, *Electromagnetic Waves* (Van Nostrand, New York, 1943).
25. W. M. Elsasser, "Attenuation in a dielectric circular rod," J. Appl. Phys. **20,** 1193–1196 (1949).
26. L. Reiffel and N. S. Kapany, "Some considerations on luminescent fiber chambers and intensifier screens," Rev. Sci. Instrum. **31,** 1136–1139 (1960).
27. N. S. Kapany and D. F. Capellaro, "Fiber optics. Image transfer from Lambertian emitters," J. Opt. Soc. Am. **51,** 23–31 (1961).
28. N. S. Kapany and J. J. Burke, "Fiber optics. Waveguide effects," J. Opt. Soc. Am. **51,** 1067–1078 (1961).
29. N. S. Kapany, J. J. Burke, and C. C. Shaw, "Fiber optics. Evanescent boundary wave propagation," J. Opt. Soc. Am. **53,** 929–935 (1963).
30. R. J. Potter, "Transmission of optical fibers," J. Opt. Soc. Am. **51,** 1079–1089 (1961).
31. R. J. Potter, "Light collecting properties of a perfect circular optical fiber," J. Opt. Soc. Am. **53,** 256–260 (1963).
32. R. Ulrich and W. Prettl, "Planar leaky light guides and couplers," Appl. Phys. **1,** 55–68 (1973).
33. A. Reisinger, "Characteristics of optical guided modes in lossy waveguides," Appl. Opt. **12,** 1015–1025 (1973).
34. G. Muller, K. Abraham, and M. Schaldach, "Quantitative ATR spectroscopy: some basic considerations," Appl. Opt. **20,** 1182–1190 (1981).
35. D. Marcuse, "Scattering and absorption losses of multimode optical fibers and fiber lasers," Bell Syst. Tech. J. **55,** 1463–1488 (1976).
36. A. W. Snyder and J. D. Love, *Optical Waveguide Theory* (Chapman & Hall, London, 1983).
37. V. Ruddy, "An effective attenuation coefficient for evanescent-wave spectroscopy using multimode fiber," Fiber Int. Opt. **9,** 143–151 (1990).
38. V. Ruddy, B. D. MacCraith, and J. A. Murphy, "Evanescent wave absorption spectroscopy using multimode fibers," J. Appl. Phys. **67,** 6070–6074 (1990).
39. B. D. Gupta, C. D. Singh, and A. Sharma, "Fiber-optic evanescent field absorption sensor: effect of launching condition and the geometry of the sensing region," Opt. Eng. **33,** 1864–1868 (1994).